

# CONCOLOR: Constrained Non-Convex Low-Rank Model for Image Deblocking

Jian Zhang, *Member, IEEE*, Ruiqin Xiong, *Member, IEEE*, Chen Zhao, Yongbing Zhang, Siwei Ma, *Member, IEEE*, and Wen Gao, *Fellow, IEEE*

**Abstract**—Due to independent and coarse quantization of transform coefficients in each block, block-based transform coding usually introduces visually annoying blocking artifacts at low bitrates, which greatly prevents further bit reduction. To alleviate the conflict between bit reduction and quality preservation, deblocking as a post-processing strategy is an attractive and promising solution without changing existing codec. In this paper, in order to reduce blocking artifacts and obtain high-quality image, image deblocking is formulated as an optimization problem within maximum *a posteriori* framework, and a novel algorithm for image deblocking using constrained non-convex low-rank model is proposed. The  $l_p$  ( $0 < p < 1$ ) penalty function is extended on singular values of a matrix to characterize low-rank prior model rather than the nuclear norm, while the quantization constraint is explicitly transformed into the feasible solution space to constrain the non-convex low-rank optimization. Moreover, a new quantization noise model is developed, and an alternatively minimizing strategy with adaptive parameter adjustment is developed to solve the proposed optimization problem. This parameter-free advantage enables the whole algorithm more attractive and practical. Experiments demonstrate that the proposed image deblocking algorithm outperforms the current state-of-the-art methods in both the objective quality and the perceptual quality.

**Index Terms**—Image deblocking, low-rank, blocking artifact reduction, optimization, quantization constraint.

## I. INTRODUCTION

RECENT years have witnessed the rapid developments of social network and mobile internet, and image and video have been becoming the main carrier of multimedia. For image and video compression, block-based transform

Manuscript received August 11, 2015; revised November 29, 2015; accepted December 21, 2015. Date of publication January 8, 2016; date of current version January 29, 2016. This work was supported by the National Basic Research Program of China (Grant 2015CB351800), the Post-Doctoral Science Foundation of China (Grant 2015M580018), the National Natural Science Foundation of China (Grant 61322106, 61370114, 61421062, 61572047, U1201255, and U1301257), the Shenzhen Peacock Plan, and also by the Cooperative Medianet Innovation Center. The associate editor coordinating the review of this manuscript and approving it for publication was Prof. Lei Zhang. (*Corresponding author: Ruiqin Xiong.*)

J. Zhang, R. Xiong, C. Zhao, S. Ma, and W. Gao are with the Institute of Digital Media, School of Electronics Engineering and Computer Science, Peking University, Beijing 100871, China (e-mail: jian.zhang@pku.edu.cn; rqxiong@pku.edu.cn; zhaochen@pku.edu.cn; swma@pku.edu.cn; wgao@pku.edu.cn).

Y. Zhang is with the Shenzhen Key Laboratory of Broadband Network and Multimedia, Graduate School at Shenzhen, Tsinghua University, Shenzhen 518055, China (e-mail: zhang.yongbing@sz.tsinghua.edu.cn).

Color versions of one or more of the figures in this paper are available online at <http://ieeexplore.ieee.org>.

Digital Object Identifier 10.1109/TIP.2016.2515985

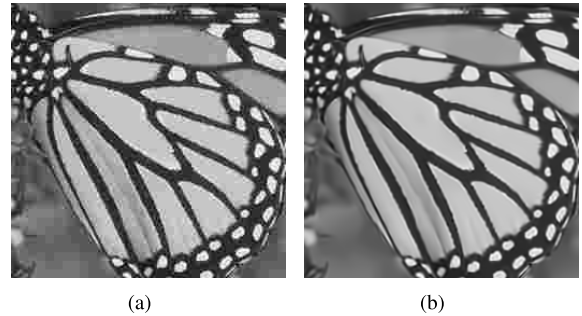


Fig. 1. Illustrations for blocking artifacts and image deblocking with respect to *Butterfly*. (a) JPEG-coded image with 0.54 bpp (PSNR = 25.24 dB); (b) Deblocking result of (a) using the proposed image deblocking algorithm (PSNR = 27.90 dB). Obviously, (b) has much better quality than (a).

coding has been widely adopted in various current coding standards, such as JPEG [1], H.264/AVC [2], and H.265/HEVC [3], due to its regularity and simplicity for hardware implementation. Among all the transform kernels, block discrete cosine transform (BDCT) is the most popular one owing to its good energy compaction and de-correlation properties. However, due to independent and coarse quantization of discrete cosine transform (DCT) coefficients in each block, BDCT coding technique usually results in visually annoying blocking artifacts in coded images and videos, especially at low bitrates, which greatly prevents further bit reduction. As illustrated in Fig. 1(a), the blocking artifacts are characterized by visually noticeable discontinuity between neighboring blocks.

The procedure to effectively remove the blocking artifacts and obtain visually acceptable quality for BDCT coded images and videos is referred to as image/video deblocking, which has attracted great interest of researchers [4]–[25]. This paper mainly focuses on image deblocking for JPEG-coded images. In order to alleviate the conflict between bit reduction and image quality preservation while maintaining standard compliant, image deblocking as a post-processing technique becomes an attractive and promising solution due to its advantage of requiring no change of existing codec. Remarkably reducing blocking artifacts is able to improve image quality with respect to a specific bit rate of compression. For instance, JPEG-coded image of *Butterfly* with 0.54 bpp is shown in Fig. 1(a). Fig. 1(b) is the deblocking result of Fig. 1(a) using the proposed image deblocking algorithm. Obviously, Fig. 1(b) has much better quality than (a), preserving visually acceptable quality while being standard compliant.

In recent years, researchers have developed a number of post-processing methods for image deblocking, which can be generally divided into two categories [4], [5]: image enhancement based deblocking methods and image restoration based deblocking methods. The basic idea of image enhancement based deblocking methods is to consider deblocking as an image enhancement process, and to conduct filtering in spatial and frequency domain to smooth visible artifacts. Zhai *et al.* proposed an effective deblocking method for JPEG compressed image through post-filtering in shifted windows of image blocks [6]. Zhai *et al.* also developed an image deblocking method involving three parts: i.e., local AC coefficient regularization in the DCT domain, block-wise shape adaptive filtering in the spatial domain, and quantization constraint in the DCT domain [7]. Foi *et al.* developed an image deblocking filtering based on shape-adaptive DCT, in conjunction with the anisotropic local polynomial approximation-intersection of confidence intervals technique, which defines the shape of the transforms support in a pointwise adaptive manner [8]. Inspired by the success of nonlocal means and bilateral filter for image denoising, some nonlocal filters to have been proposed for image deblocking [9]–[11]. Farinella *et al.* exploited the Structure Sparse Coding Model Selection (SSMS) to restore compressed noisy images, yielding impressive performance improvement [12]. Kim proposed an adaptive image blocking artifact reduction method by exploiting the directional activity of wavelet-based block analysis [13]. Lately, Yoo *et al.* proposed to classify the coded image into flat region and edge region, and developed a two-step framework for reducing blocking artifacts in different region based on inter-block correlation [14]. Yeh *et al.* proposed a self-learning-based post-processing framework for image/video deblocking by formulating deblocking as a morphological component analysis based image decomposition problem via sparse representation [5].

For image restoration based deblocking methods, deblocking is usually formulated as an ill-posed image inverse problem by exploiting some image prior knowledge and observed data at the decoder [15]. For instance, iterative image recovery algorithms were proposed using the traditional projection onto convex sets (POCS) [16]–[19]. Total variation [20], block-based sparse representation [21]–[23], Markov random field (MRF) [24], [25] were utilized as image prior models to seek the MAP estimation of the original image. Typically, Sun and Cham modeled the quantization distortion as Gaussian noise, and used field of experts as image prior to construct image deblocking optimization problem [26]. Recently, Zhang *et al.* proposed to utilize image block similarity prior model to reduce compression artifacts by the overlapped block transform coefficient estimation from non-local blocks [27], [28].

From above previous works, it can be inferred that image prior models play an important role in both image enhancement based deblocking methods and image restoration based deblocking methods. The evolution of image prior models is from local to nonlocal, and from pixel-wise to block-wise [29]–[32]. Recent studies show that, by exploiting the non-local self-similarity and clustering similar blocks,

low-rank prior models achieve promising results in image restoration tasks, such as image deblocking [33], [34] and image denoising [35]–[37].

However, there exist two issues in current image deblocking strategies with low-rank models [33], [34]. First, to obtain an approximated solution, they both adopt the nuclear norm (sum of the singular values) as a convex surrogate of the matrix rank. Despite good theoretical guarantee by the classic technique of singular value thresholding (SVT) [38], [39], the nuclear norm is actually not accurate enough to approximate the matrix rank. Second, they neither take quantization constraint (QC) into account, which means that the DCT coefficients of the deblocking image do not always lie within the quantization limits defined by the compression.

In this paper, to deal with the above two issues, we extend the surrogate function of  $l_0$  norm, i.e.  $l_p$  ( $0 < p < 1$ ) penalty function on singular values of a matrix to substitute for the nuclear norm for characterizing low-rank prior model. Inspired by the success of  $l_p$  ( $0 < p < 1$ ) sparse optimization, the proposed non-convex low-rank model is expected to be more accurate than traditional nuclear norm. In addition, quantization constraint is transformed into the feasible solution space, which is explicitly used to constrain the non-convex low-rank optimization. Therefore, a novel **CON**strained **NON-CON**vex **LOW-R**ank (CONCOLOR) model is proposed for image deblocking. Moreover, a new quantization noise model is developed, and the proposed objective function is efficiently solved by the alternatively minimizing strategy. It is worth emphasizing that the proposed image deblocking algorithm CONCOLOR is parameter-adaptive, which enables the whole algorithm more effective and attractive. Extensive experiments manifest that the proposed image deblocking algorithm outperforms current state-of-the-art algorithms in both PSNR and visual perception, and greatly improves current existing image deblocking quality.

The remainder of this paper is organized as follows. The background of JPEG compression and decompression and some notations are given in Section II. Section III elaborates the proposed image deblocking framework. Section IV presents the implementation details of solving the proposed optimization problem. Extensive experimental results are reported in Section V. In Section VI, we conclude this paper.

## II. BACKGROUND

In this section, we briefly review the process of JPEG compression and decompression, and give some notations for the convenience of later discussions.

It is known that JPEG is able to generate acceptable compressed images at a rather high compression with very easy implementation, rendering it one of the most popular lossy compression schemes in the last two decades. Basically, JPEG compression is composed of four stages: a) split the whole input image into non-overlapped blocks of size  $8 \times 8$ ; b) apply discrete cosine transformation (DCT) on each block; c) divide DCT coefficients of each block by a quantization table element-wisely and round the quantized values; d) use entropy coding to generate the JPEG compressed bit-stream.

The JPEG decompression is inverse, which involves lossless entropy decoding, de-quantization, inverse DCT (IDCT) to each block, and block reassembling. It is obvious to see that the information loss for JPEG compression takes place in the stage of quantization, leading to round-off errors in each block, which inevitably produces blocking artifacts.

In this paper, the boldface uppercase letters denote matrices, e.g.  $\mathbf{X}$ , and  $\mathbf{X}_{[i,j]}$  is defined as the  $(i, j)^{th}$  entry of matrix  $\mathbf{X}$ . The boldface lowercase letters denote column vectors, e.g.  $\mathbf{x}$ , and  $\mathbf{x}_{[k]}$  is defined as the  $k^{th}$  entry of vector  $\mathbf{x}$ . Italics denotes scalars.  $\|\mathbf{x}\|_0$  counts the nonzero elements in  $\mathbf{x}$ , and  $\|\mathbf{X}\|_F$  denotes the Frobenius norm of  $\mathbf{X}$ . Suppose we have an image  $\mathbf{X}$  of size  $N \times N$ . Then its vector representation is  $\mathbf{x}$ , and  $\mathbf{x}_{[(i-1) \times N + j]}$  stands for the pixel with the coordinates in the vertical and the horizontal directions being  $i$  and  $j$  in image  $\mathbf{X}$ , respectively. Here, to simplify the first two stages of JPEG compression, like [23], let us define a block DCT  $N \times N$  matrix operator  $\mathcal{A}$ , which can transform each non-overlapped  $8 \times 8$  block of the input image to its frequency domain. Similarly, the matrix operator  $\mathcal{A}^{-1}$  represents the inverse process. The quantization matrix of size  $8 \times 8$  is denoted by  $\mathbf{M}^q$ , determined by the quality factor (QF)  $q$  in the range [1 100]. Suppose  $\mathbf{x}$  is the original image and let  $\mathbf{y}$  be the observed JPEG-coded image which is directly decompressed from the JPEG compressed bit-stream by JPEG decoder. Denote

$$\hat{\mathbf{x}} = \mathcal{A}\mathbf{x}; \quad \hat{\mathbf{y}} = \mathcal{A}\mathbf{y}, \quad (1)$$

which stand for the frequency images of  $\mathbf{x}$  and  $\mathbf{y}$ , respectively.

Then, according to the process of JPEG compression described above, we have

$$\hat{\mathbf{y}}_{[(k-1) \times N + l]} = \text{round} \left( \frac{\hat{\mathbf{x}}_{[(k-1) \times N + l]}}{\mathbf{M}_{[k,l]}} \right) \times \mathbf{M}_{[k,l]}, \quad (2)$$

where  $1 \leq k, l \leq N$ ,  $\text{round}(\cdot)$  is to round towards the nearest integer,  $\mathbf{M}$  is a matrix of size  $N \times N$  with  $\mathbf{M}_{[k,l]} = \mathbf{M}_{[\bar{k}, \bar{l}]}$ , and  $\bar{k} = \text{mod}(k, 8)$ ;  $\bar{l} = \text{mod}(l, 8)$ .

The purpose of image deblocking is to take advantage of the information in JPEG compressed bit-stream, such as  $\mathbf{y}$  and  $\mathbf{M}^q$ , to suppress blocking artifacts and obtain a high-quality reconstruction image.

### III. CONSTRAINED NON-CONVEX LOW-RANK (CONCOLOR) MODEL FOR IMAGE DEBLOCKING

In this paper, we cast image deblocking as an image inverse problem, and formulate the proposed algorithm through maximum a posteriori (MAP) framework. Thus, our proposed algorithm belongs to the category of image restoration based deblocking method.

To be concrete, given JPEG compressed image  $\mathbf{y}$ , the original image  $\mathbf{x}$  can be obtained by

$$\tilde{\mathbf{x}} = \arg \max_{\mathbf{x}} p(\mathbf{x}|\mathbf{y}). \quad (3)$$

According to the Bayesian rule, the above problem Eq. (3) can be expressed as

$$\tilde{\mathbf{x}} = \arg \max_{\mathbf{x}} \log(p(\mathbf{y}|\mathbf{x})) + \log(p(\mathbf{x})), \quad (4)$$

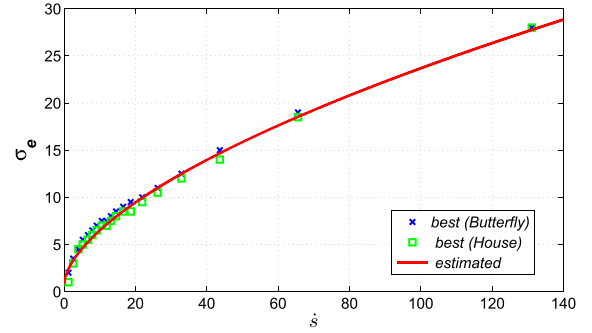


Fig. 2. Agreement between the values of  $\sigma_e$  estimated by Eq. (6) and the optimal ones (found experimentally), which give the highest PSNR for the deblocking *Butterfly* and *House* images using our proposed algorithm.

where the first term in Eq. (4) represents data-fidelity, characterizing the relationship between  $\mathbf{y}$  and  $\mathbf{x}$ , and the second term corresponds to the image prior knowledge constraining the solution space. In this paper, a new quantization noise model is developed to depict  $\log(p(\mathbf{y}|\mathbf{x}))$ , and a new constrained non-convex low-rank model is formulated to interpret  $\log(p(\mathbf{x}))$ . Hence, a novel constrained non-convex low-rank minimization function for image deblocking is proposed. The details are provided in the following.

#### A. Quantization Noise Model

In the literature, the observed JPEG-coded image is usually modelled as the corrupted one by the quantization noise, i.e.

$$\mathbf{y} = \mathbf{x} + \mathbf{e}, \quad (5)$$

where  $\mathbf{y}$  is the JPEG-coded image with blocking artifacts,  $\mathbf{x}$  is the original image, and  $\mathbf{e}$  is the quantization noise. Many sophisticated models of BDCT quantization noise have been proposed [8], [25], [26], [40], [41].

In this paper, we adopt Gaussian model to characterize the quantization noise  $\mathbf{e}$  in Eq. (5) due to its simplicity and effectiveness. To estimate its variance  $\sigma_e^2$  that is suitable for our proposed framework, we first observe the optimal values of  $\sigma_e$  found experimentally for the images *Butterfly* and *House* compressed with different quantization tables  $\mathbf{M}^q$  corresponding to quality factor  $q = 5, 10, \dots, 95$ , as illustrated in Fig. 2. It can be inferred that different images with the same  $q$  have similar optimal values of  $\sigma_e$ , which means that  $\sigma_e$  is only related with  $q$ . Hence, in this paper, we propose to estimate the optimal value of  $\sigma_e$  directly from the quantization table  $\mathbf{M}^q$  by curve fitting using the following empirical formulation:

$$\sigma_e^2 = 1.195 * (\hat{s})^{0.6394} + 0.9693, \quad \hat{s} = \frac{1}{9} \sum_{i,j=1}^3 \mathbf{M}_{[i,j]}^q, \quad (6)$$

where  $\mathbf{M}^q$  is the  $8 \times 8$  quantization matrix with the quality factor  $q$ , and  $\hat{s}$  is the mean value of the nine upper-left entries in  $\mathbf{M}^q$ , corresponding to the lowest-frequency DCT harmonics. It is apparent that a higher compression corresponds to a larger value for the variance.

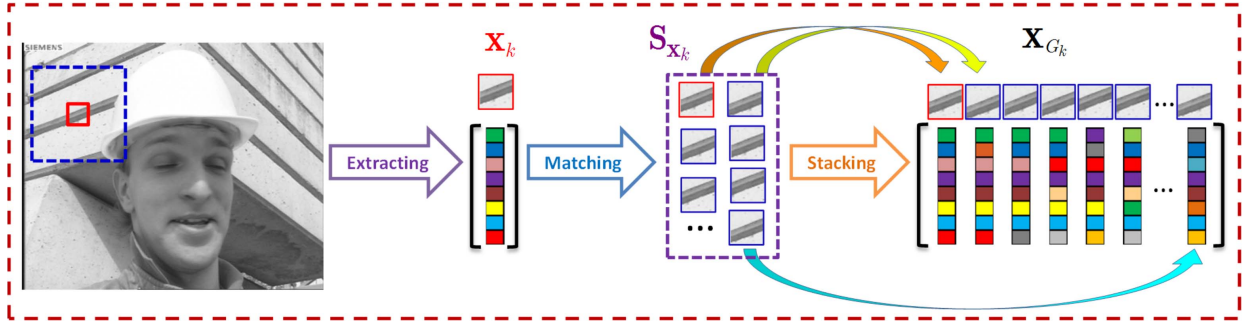


Fig. 3. Illustrations for image low-rank prior. Extract each exemplar patch vector  $\mathbf{x}_k$  from image  $\mathbf{x}$ . For each  $\mathbf{x}_k$ , denote  $\mathbf{S}_{\mathbf{x}_k}$  the set composed of its best matched blocks. Stack all the patches in  $\mathbf{S}_{\mathbf{x}_k}$  to construct the data matrix, denoted by  $\mathbf{X}_{G_k}$ .  $\mathbf{X}_{G_k}$  has a low-rank property.

With the Gaussian quantization noise model, the first data-fidelity term in Eq. (4) thus can be formulated as

$$\log(p(\mathbf{y}|\mathbf{x})) = -\frac{1}{2\sigma_{\epsilon}^2} \|\mathbf{x} - \mathbf{y}\|_2^2. \quad (7)$$

Note that  $\sigma_{\epsilon}^2$  in Eq. (7) is adaptively determined by Eq. (6) according to different quantization matrices. Experiments for a wide range of different quantization matrices in Section V will verify the robustness and effectiveness of Gaussian quantization noise model and Eq. (6). Here, it is also worth emphasizing that the noise variance  $\sigma_{\epsilon}^2$  calculated by Eq. (6) is not the real estimate of the variance of the difference between the original and the compressed images. Under the assumption of Gaussian noise model, it is just the variance of the hypothetical Gaussian noise, which determines the level of adaptive smoothing that is able to reduce the artifacts generated by the BDCT quantization with  $\mathbf{M}^q$  [8].

### B. Non-Convex Low-Rank Prior

In this section, we will elaborate the proposed non-convex low-rank prior model.

The basic assumption is that the well-known non-local self-similarity, which depicts the repetitiveness of higher level patterns (e.g. textures and structures) globally positioned in natural images, implies that many similar patches can be searched for any exemplar patch [42], [43]. To be concrete, as illustrated in Fig. 3, first, divide the image  $\mathbf{x} \in \mathbb{R}^{N^2}$  with size  $N^2$  into  $K$  overlapped patches of size  $\sqrt{B_s} \times \sqrt{B_s}$ , and each patch is denoted by the vector  $\mathbf{x}_k \in \mathbb{R}^{B_s}$ , i.e.  $k = 1, 2, \dots, K$ . Then, for each exemplar patch  $\mathbf{x}_k$ , denoted by small red square in Fig. 3, within the  $W_s \times W_s$  training window (big blue square), search its  $c$  best matched patches, which comprise the group  $\mathbf{S}_{\mathbf{x}_k}$ . Here, Euclidean distance is selected as the similarity criterion between different patches. Next, all the patches in each group  $\mathbf{S}_{\mathbf{x}_k}$  are stacked into a data matrix of size  $B_s \times c$ , denoted by  $\mathbf{X}_{G_k}$ , which includes every patch in  $\mathbf{S}_{\mathbf{x}_k}$  as its columns, i.e.  $\mathbf{X}_{G_k} = [\mathbf{x}_{G_k} \otimes 1, \mathbf{x}_{G_k} \otimes 2, \dots, \mathbf{x}_{G_k} \otimes c]$ . Since all the patches in each data matrix have similar structures, the constructed data matrix  $\mathbf{X}_{G_k}$  has a low-rank property. In practice, we usually suppose  $\mathbf{X}_{G_k}$  is corrupted by some noise. As discussed in Section III.A, we can model the data matrix as:  $\mathbf{X}_{G_k} = \mathbf{Z}_{G_k} + \mathbf{S}_{G_k}$ , where  $\mathbf{Z}_{G_k}$  and  $\mathbf{S}_{G_k}$  denote the low-rank matrix and the Gaussian noise matrix, respectively.

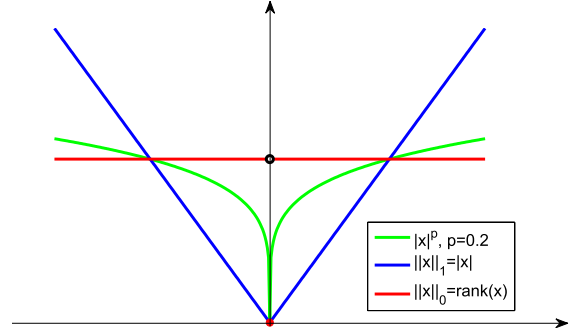


Fig. 4. Illustrations of  $F(x) = |x|^p$ , ( $0 < p < 1$ ) (green),  $rank(x) = \|x\|_0$  (red), and the nuclear norm  $\|x\|_1$  (blue) in the case of a scalar.

Then, the low-rank matrix  $\mathbf{Z}_{G_k}$  can be reconstructed by solving the following optimization problem:

$$\mathbf{Z}_{G_k} = \arg \min \frac{1}{2\sigma_s^2} \|\mathbf{X}_{G_k} - \mathbf{Z}_{G_k}\|_F^2 + \lambda rank(\mathbf{Z}_{G_k}). \quad (8)$$

where  $\|\cdot\|_F^2$  denotes the Frobenious norm and  $\sigma_s^2$  denotes the variance of additive Gaussian noise. In general, the rank minimization is an NP-hard problem. To obtain an approximated solution, the nuclear norm (sum of the singular values) is usually adopted as a convex surrogate of the rank. By the nuclear norm, the rank minimization problem can be efficiently solved by the classic technique of singular value thresholding (SVT) [39]. Despite the good theoretical guarantee, the nuclear norm is actually not accurate to approximate the rank, as shown in Fig. 4.

Inspired by the success of  $l_p$  ( $0 < p < 1$ ) sparse optimization, in this paper, to approximate matrix rank more accurately, we extend the non-convex  $l_p$  ( $0 < p < 1$ ) penalty function on singular values of the data matrix to substitute the convex nuclear norm. Concretely, the rank function can be approximately solved by the following function:

$$F(\mathbf{Z}_{G_k}) = \sum_{i=1}^c |\sigma_i(\mathbf{Z}_{G_k})|^p, \quad (9)$$

where  $0 < p < 1$  and  $\sigma_i(\mathbf{X})$  denotes the  $i$ -th singular value of a matrix  $\mathbf{X} \in \mathbb{R}^{B_s \times c}$  (assuming  $B_s \leq c$  in this work). Fig. 4 shows the comparison of the proposed non-convex surrogate function  $F(\mathbf{Z}_{G_k})$ , the rank, and the nuclear norm in the scalar case. One can clearly see that the proposed  $F(\mathbf{Z}_{G_k})$

is more accurate to approximate the rank than the nuclear norm.

Therefore, for each exemplar image patch, we can approximate the matrix  $\mathbf{X}_{G_k}$  with a low-rank matrix  $\mathbf{Z}_{G_k}$  by solving the following minimization instead of Eq. (8):

$$\mathbf{Z}_{G_k} = \arg \min_{\mathbf{Z}_{G_k}} \frac{1}{2\sigma_s^2} \|\mathbf{X}_{G_k} - \mathbf{Z}_{G_k}\|_F^2 + \lambda F(\mathbf{Z}_{G_k}). \quad (10)$$

Accordingly, considering all the matrices  $\mathbf{X}_{G_k}$ , the proposed non-convex low-rank prior model is formulated as

$$\log(p(\mathbf{x})) = -\left( \frac{\alpha}{2\sigma_s^2} \sum_{k=1}^K \|\mathbf{R}_{G_k} \mathbf{x} - \mathbf{Z}_{G_k}\|_F^2 + \beta \sum_{k=1}^K F(\mathbf{Z}_{G_k}) \right), \quad (11)$$

where  $\mathbf{X}_{G_k} = \mathbf{R}_{G_k} \mathbf{x} = [\mathbf{x}_{G_k} \otimes 1, \mathbf{x}_{G_k} \otimes 2, \dots, \mathbf{x}_{G_k} \otimes c]$  is the matrix operator that extracts the patch  $\mathbf{x}_{G_k} \otimes i$  from  $\mathbf{x}$ . Obviously, the proposed non-convex low-rank model is able to exploit both the non-local self-similarity of similar patches and non-convexity of rank minimization simultaneously, which is expected to achieve better recovery than previous methods.

### C. Quantization Constraint Prior

For image deblocking problem, the quantization constraint (QC) is a key prior [26], which is unfortunately ignored by current algorithms with low-rank approximation [33], [34]. Considering the quantization step in JPEG compression, we incorporate QC into the proposed framework.

Firstly, the quantization step in Eq. (2) can be equivalently transformed into

$$\left| \frac{\hat{\mathbf{x}}_{[(k-1) \times N+1]} - \hat{\mathbf{y}}_{[(k-1) \times N+1]}}{\mathbf{M}_{[k,l]}} \right| \leq \omega, \quad (12)$$

where  $1 \leq k, l \leq N$ , and  $\omega$  is usually set to be not more than 0.5 [19].

Next, Eq. (12) is expanded as

$$\begin{aligned} & (\hat{\mathbf{y}}_{[(k-1) \times N+1]} - \omega \times \mathbf{M}_{[k,l]}) \\ & \leq \hat{\mathbf{x}}_{[(k-1) \times N+1]} \leq (\hat{\mathbf{y}}_{[(k-1) \times N+1]} + \omega \times \mathbf{M}_{[k,l]}). \end{aligned} \quad (13)$$

Let us define the lower and upper bound vectors  $\hat{\mathbf{l}}$  and  $\hat{\mathbf{u}}$ , i.e.

$$\begin{aligned} \hat{\mathbf{l}}_{[(k-1) \times N+1]} &= (\hat{\mathbf{y}}_{[(k-1) \times N+1]} - \omega \times \mathbf{M}_{[k,l]}); \\ \hat{\mathbf{u}}_{[(k-1) \times N+1]} &= (\hat{\mathbf{y}}_{[(k-1) \times N+1]} + \omega \times \mathbf{M}_{[k,l]}). \end{aligned} \quad (14)$$

Therefore, as illustrated in Fig. 5, the frequency coefficients of the original image should satisfy

$$\hat{\mathbf{l}} \preceq \hat{\mathbf{x}} \preceq \hat{\mathbf{u}}, \quad (15)$$

where  $\preceq$  denotes the operator of element-wise comparison. Eq. (15) is just the expression of QC. Furthermore, the solution space restricted by QC can be defined as

$$\Omega = \{\mathbf{x} | \hat{\mathbf{l}} \preceq \mathbf{Ax} \preceq \hat{\mathbf{u}}\}. \quad (16)$$

Note that  $\Omega$  can be directly obtained from the given JPEG compressed bit-stream. As to image enhancement based deblocking methods, the most commonly way is to apply QC

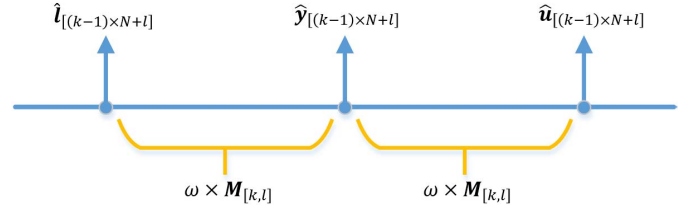


Fig. 5. Illustrations for quantization constraint in JPEG compression. The original frequency coefficient  $\hat{\mathbf{x}}_{[(k-1) \times N+1]}$  lies in the range between  $\hat{\mathbf{l}}_{[(k-1) \times N+1]}$  and  $\hat{\mathbf{u}}_{[(k-1) \times N+1]}$ .

to restrain the final deblocking result to improve the performance. However, this does not always work for image restoration based deblocking methods. In this paper, we explicitly incorporate the feasible solution space  $\Omega$  into Eq. (4), and design a novel constrained optimization problem. Furthermore, in order to make better use of QC prior, different from previous work [16], [23], we exploit narrow quantization constraint (NQC) [19] to construct the feasible solution space  $\Omega$  by setting  $\omega$  in Eq. (14) to be 0.4, instead of 0.5. The advantage of  $\omega = 0.4$  over  $\omega = 0.5$  for the proposed algorithm will be presented in the experimental section.

### D. Proposed Image Deblocking Framework

Incorporating the above quantization noise model and two image priors into Eq. (4), we have the proposed novel CONstrained Non-CONvex LOW-Rank (CONCOLOR) optimization problem as follows

$$\begin{aligned} (\tilde{\mathbf{x}}, \tilde{\mathbf{Z}}_{G_k}) &= \arg \min_{\mathbf{x}, \mathbf{Z}_{G_k}} \frac{1}{2\sigma_e^2} \|\mathbf{x} - \mathbf{y}\|_F^2 + \frac{\alpha}{2\sigma_s^2} \sum_{k=1}^K \|\mathbf{R}_{G_k} \mathbf{x} - \mathbf{Z}_{G_k}\|_F^2 \\ &+ \beta \sum_{k=1}^K F(\mathbf{Z}_{G_k}) \quad s.t. \quad \mathbf{x} \in \Omega. \end{aligned} \quad (17)$$

Compared with existing image deblocking algorithms with low-rank priors [33], [34], there are three main improvements in CONCOLOR. The first one is the introduction of the non-convex low-rank approximation function  $F(\mathbf{Z}_{G_k})$  by extending  $l_p$  ( $0 < p < 1$ ) on the singular values of a matrix, which is more accurate than the convex nuclear norm. The second one is that narrow quantization constraint is explicitly used to construct the feasible solution space  $\Omega$  as the optimization constraint, which will be verified quite effective for image deblocking. The third one is that an alternatively minimizing strategy with adaptive parameter adjustment is developed to solve the proposed optimization problem. The parameter-free advantage enables the whole algorithm more attractive and practical. More details about the optimization will be provided in the next section. Note that Eq. (17) jointly exploits the quantization model, low-rank prior and QC prior within the MAP framework. Thus, it is expected that better deblocking results will be achieved.

## IV. ALGORITHM OPTIMIZATION AND PARAMETER SETTING FOR CONCOLOR

In this section, we will show how to utilize the alternatively minimizing strategy to solve the proposed optimization

problem (17) efficiently with respect to the whole image  $\mathbf{x}$  and low-rank data matrices  $\mathbf{Z}_{G_k}$ .

#### A. Non-Convex Low-Rank Minimization

Given  $\mathbf{x}$ , the non-convex low-rank minimization for each  $\mathbf{Z}_{G_k}$  ( $k = 1, \dots, K$ ) is formulated as:

$$\tilde{\mathbf{Z}}_{G_k} = \arg \min_{\mathbf{Z}_{G_k}} \frac{\alpha}{2\sigma_s^2} \|\mathbf{R}_{G_k} \mathbf{x} - \mathbf{Z}_{G_k}\|_F^2 + \beta \sum_{k=1}^K F(\mathbf{Z}_{G_k}). \quad (18)$$

Let  $\tau = \frac{\sigma_s^2 \beta}{\alpha}$ , then we get

$$\min \frac{1}{2} \|\mathbf{X}_{G_k} - \mathbf{Z}_{G_k}\|_F^2 + \sum_{i=1}^c g_\tau(\sigma_i(\mathbf{Z}_{G_k})), \quad (19)$$

where the penalty function  $g_\tau(\cdot)$  is defined as  $g_\tau(x) = \tau|x|^p$ , ( $0 < p < 1$ ).

Note that  $g_\tau(x)$  is concave and monotonically increasing on  $[0, \infty)$ , with its gradients being decreasing. Based on this property, recently, Lu *et al.* proposed an iteratively reweighted nuclear norm (IRNN) algorithm to solve the general non-convex non-smooth low-rank minimization with convergence guarantee [44]. Here, borrowing the wisdom of IRNN, we will show how to solve the problem (19).

For simplicity of notation, denote  $h(\mathbf{Z}_{G_k}) = \frac{1}{2} \|\mathbf{X}_{G_k} - \mathbf{Z}_{G_k}\|_F^2$ ,  $\sigma_i = \sigma_i(\mathbf{Z}_{G_k})$ , and  $\sigma_i^{(l)} = \sigma_i(\mathbf{Z}_{G_k}^{(l)})$ . Owing to that  $g_\tau(x)$  is concave and differentiable on  $[0, \infty)$ , we obtain

$$g_\tau(\sigma_i) \leq g_\tau(\sigma_i^{(l)}) + w_i^{(l)}(\sigma_i - \sigma_i^{(l)}). \quad (20)$$

Here

$$w_i^{(l)} = g'_\tau(\sigma_i^{(l)}), \quad (21)$$

$g'_\tau(x) = \tau p x^{p-1}$ ,  $x \in [0, \infty)$ .

Then, by the anti-monotone gradient property of  $g_\tau(x)$ , since  $\sigma_1^{(l)} \geq \sigma_2^{(l)} \geq \dots \geq \sigma_c^{(l)} \geq 0$ , we have

$$0 \leq w_1^{(l)} \leq w_2^{(l)} \leq \dots \leq w_c^{(l)}. \quad (22)$$

The property (22) is very important for achieving efficient solution to (19), which will be shown later. According to (20), we minimize its right hand instead of  $g_\tau(\sigma_i)$ , leading to the following relaxed problem

$$\mathbf{Z}_{G_k}^{(l+1)} = \arg \min_{\mathbf{Z}_{G_k}} g_\tau(\sigma_i^{(l)}) + w_i^{(l)}(\sigma_i - \sigma_i^{(l)}) + h(\mathbf{Z}_{G_k}). \quad (23)$$

Removing the constant terms, the problem (23) equivalently becomes

$$\mathbf{Z}_{G_k}^{(l+1)} = \arg \min_{\mathbf{Z}_{G_k}} w_i^{(l)}(\sigma_i(\mathbf{Z}_{G_k})) + h(\mathbf{Z}_{G_k}). \quad (24)$$

Furthermore, instead of updating  $\mathbf{Z}_{G_k}^{(l+1)}$  by solving (24) directly, we linearize  $h(\mathbf{Z}_{G_k})$  at  $\mathbf{Z}_{G_k}^{(l)}$  and add a proximal term:

$$h(\mathbf{Z}_{G_k}) \approx h(\mathbf{Z}_{G_k}^{(l)}) + \langle \nabla h(\mathbf{Z}_{G_k}^{(l)}), \mathbf{Z}_{G_k} - \mathbf{Z}_{G_k}^{(l)} \rangle + \frac{\mu}{2} \|\mathbf{Z}_{G_k} - \mathbf{Z}_{G_k}^{(l)}\|_F^2, \quad (25)$$

---

#### Algorithm 1 Solving Non-Convex Low-Rank Problem (19)

---

- 1: **Input:**  $\mu$
  - 2: **Initialization:**  $t = 0, \mathbf{Z}_{G_k}^{(0)}, w_i^{(0)}, i = 1, \dots, c$
  - 3: **For**  $l = 1, \dots, L$
  - 4:   Update  $\mathbf{Z}_{G_k}^{(l)}$  by solving problem (27) with (29);
  - 5:   Update the weights  $w_i^{(l)}$  by  $w_i^{(l)} = g'_\tau(\sigma_i(\mathbf{Z}_{G_k}^{(l)}))$ .
  - 6: **End For**
  - 7: **Output:** The solution to (19), i.e.  $\tilde{\mathbf{Z}}_{G_k} = \mathbf{Z}_{G_k}^{(L)}$
- 

where  $\mu > L(h)$ , and  $L(h) > 0$  is the Lipschitz constant of  $\nabla h$ . Hence, the update of  $\mathbf{Z}_{G_k}^{(l+1)}$  is

$$\begin{aligned} \mathbf{Z}_{G_k}^{(l+1)} = \arg \min_{\mathbf{Z}_{G_k}} & w_i^{(l)}(\sigma_i(\mathbf{Z}_{G_k})) + h(\mathbf{Z}_{G_k}^{(l)}) \\ & + \langle \nabla h(\mathbf{Z}_{G_k}^{(l)}), \mathbf{Z}_{G_k} - \mathbf{Z}_{G_k}^{(l)} \rangle + \frac{\mu}{2} \|\mathbf{Z}_{G_k} - \mathbf{Z}_{G_k}^{(l)}\|_F^2, \end{aligned} \quad (26)$$

which is equivalently transformed as

$$\begin{aligned} \mathbf{Z}_{G_k}^{(l+1)} = \arg \min_{\mathbf{Z}_{G_k}} & w_i^{(l)}(\sigma_i(\mathbf{Z}_{G_k})) \\ & + \frac{\mu}{2} \|\mathbf{Z}_{G_k} - (\mathbf{Z}_{G_k}^{(l)} - \frac{1}{\mu} \nabla h(\mathbf{Z}_{G_k}^{(l)}))\|_F^2. \end{aligned} \quad (27)$$

Although (27) is still non-convex, due to the property (22), it actually has a closed-form solution based on the following Theorem 1.

*Theorem 1 [45]: For any  $\lambda > 0, \mathbf{Y} \in \mathbb{R}^{m \times n}$ , and  $0 \leq w_1 \leq w_2 \leq \dots \leq w_s$ , ( $s = \min(m, n)$ ), a globally optimal solution to the following problem*

$$\min \lambda \sum_{i=1}^s w_i \sigma_i(\mathbf{X}) + \frac{1}{2} \|\mathbf{X} - \mathbf{Y}\|_F^2, \quad (28)$$

is given by the weighted singular value thresholding

$$\mathbf{X}^* = \mathbf{U} \mathbf{S}_{\lambda w}(\Sigma) \mathbf{V}^T, \quad (29)$$

$\mathbf{Y} = \mathbf{U} \Sigma \mathbf{V}^T$  is the SVD of  $\mathbf{Y}$ , and  $\mathbf{S}_{\lambda w}(\Sigma) = \text{Diag}(\Sigma_{ii} - \lambda w_i)$ .

Therefore, by iteratively computing  $w_i^{(l)}$  according to (21) and updating  $\mathbf{Z}_{G_k}^{(l+1)}$  according to (29), we achieve the efficient solution to the non-convex low-rank minimization (19). The whole procedure to solve (19) is described in **Algorithm 1**. Moreover, **Algorithm 1** decreases the objective function value monotonically, and any limit point is a stationary point of problem (19). The convergence analysis is provided by the following Theorem 2.

*Theorem 2 [44]: The sequences  $\mathbf{Z}_{G_k}^{(l)}$  generated in Algorithm 1 satisfies the following properties:*

- 1)  $F(\mathbf{Z}_{G_k}^{(l)})$  is monotonically decreasing. Indeed,

$$F(\mathbf{Z}_{G_k}^{(l)}) - F(\mathbf{Z}_{G_k}^{(l+1)}) \geq \frac{\mu - L(h)}{2} \|\mathbf{Z}_{G_k}^{(l)} - \mathbf{Z}_{G_k}^{(l+1)}\|_F^2;$$

- 2)  $\lim_{l \rightarrow \infty} (\mathbf{Z}_{G_k}^{(l)} - \mathbf{Z}_{G_k}^{(l+1)}) = 0$ ;

- 3) The sequences  $\{\mathbf{Z}_{G_k}^{(l)}\}$  is bounded, and any accumulation point  $\tilde{\mathbf{Z}}_{G_k}$  of  $\{\mathbf{Z}_{G_k}^{(l)}\}$  is a stationary of (19).

### B. Constrained Quadratic Minimization

After obtaining each  $\mathbf{Z}_{G_k}$ , the whole image  $\mathbf{x}$  can be reconstructed by solving the following constrained quadratic minimization problem:

$$\tilde{\mathbf{x}} = \arg \min_{\mathbf{x}} \frac{1}{2\sigma_e^2} \|\mathbf{x} - \mathbf{y}\|_2^2 + \frac{\alpha}{2\sigma_s^2} \sum_{k=1}^K \|\mathbf{R}_{G_k} \mathbf{x} - \mathbf{Z}_{G_k}\|_F^2 \quad s.t. \mathbf{x} \in \Omega. \quad (30)$$

Since  $\Omega$  is convex set, to make solving (30) more efficient and tractable, we first get the solution of the unconstrained quadratic minimization of (30), and then project the solution to  $\Omega$ . Specifically, without consideration of the constraint  $\mathbf{x} \in \Omega$ , the unconstrained version of (30) is

$$\hat{\mathbf{x}} = \arg \min_{\mathbf{x}} \frac{1}{2\sigma_e^2} \|\mathbf{x} - \mathbf{y}\|_2^2 + \frac{\alpha}{2\sigma_s^2} \sum_{k=1}^K \|\mathbf{R}_{G_k} \mathbf{x} - \mathbf{Z}_{G_k}\|_F^2, \quad (31)$$

which obviously admits a closed-form solution, that is

$$\hat{\mathbf{x}} = \left( \mathbf{I} + \frac{\sigma_e^2 \alpha}{\sigma_s^2} \sum_{k=1}^K \mathbf{R}_{G_k}^T \mathbf{R}_{G_k} \right)^{-1} \left( \mathbf{y} + \frac{\sigma_e^2 \alpha}{\sigma_s^2} \sum_{k=1}^K \mathbf{R}_{G_k}^T \mathbf{Z}_{G_k} \right), \quad (32)$$

where  $\mathbf{R}_{G_k}^T \mathbf{Z}_{G_k} = \sum_{i=1}^c \mathbf{R}_{G_k}^T \otimes_i \mathbf{Z}_{G_k} \otimes_i$ ,  $\mathbf{I}$  is the identity matrix, and  $\mathbf{R}_{G_k}^T \mathbf{R}_{G_k} = \sum_{i=1}^c \mathbf{R}_{G_k}^T \otimes_i \mathbf{R}_{G_k} \otimes_i$ .

Since  $\mathbf{I} + \frac{\sigma_e^2 \alpha}{\sigma_s^2} \sum_{k=1}^K \mathbf{R}_{G_k}^T \mathbf{R}_{G_k}$  is actually a diagonal matrix, (32) can be efficiently obtained by element-wise division operations.

Next, we find the optimal feasible solution of (30) in  $\Omega$  by utilizing the projection operation, i.e.

$$\tilde{\mathbf{x}} = \mathcal{A}^{-1} \mathcal{P}(\mathcal{A}(\hat{\mathbf{x}}), \hat{\mathbf{1}}, \hat{\mathbf{u}}), \quad (33)$$

$\mathcal{A}$  is the matrix operator defined by  $\Omega$  in Section II, and  $\mathcal{P}(\mathbf{x}, \mathbf{l}, \mathbf{u})$  is a projection operator defined as

$$\mathbf{v}_{[k]} = \begin{cases} \mathbf{l}_{[k]}, & \text{if } \mathbf{x}_{[k]} < \mathbf{l}_{[k]} \\ \mathbf{x}_{[k]}, & \text{if } \mathbf{l}_{[k]} \leq \mathbf{x}_{[k]} \leq \mathbf{u}_{[k]}, \quad 1 \leq k \leq N^2. \\ \mathbf{u}_{[k]}, & \text{if } \mathbf{x}_{[k]} > \mathbf{u}_{[k]} \end{cases} \quad (34)$$

Therefore, according to (32) and (33), we can achieve the efficient solution to the constrained quadratic minimization problem (30).

To sum up, the optimization of (17) is split into two minimization sub-problems: non-convex low-rank minimization (18) and constrained quadratic minimization (30). These two minimization sub-problems are alternatively processed, and such process is iterated until the convergence.

### C. Parameter Setting

This section will give some details about parameter setting. In total, the proposed image deblocking algorithm CONCOLOR requires to tune five parameters, i.e.,  $\sigma_e^2$ ,  $\sigma_s^2$ ,  $\alpha$ ,  $\beta$ , and  $\mu$ . Among them,  $\alpha$ ,  $\beta$ , and  $\mu$  are set be fixed values, while  $\sigma_e^2$  and  $\sigma_s^2$  are adaptively adjusted depending on image content and quantization matrix.

### Algorithm 2 CONCOLOR for Image Deblocking

- 1: **Input:** JPEG compressed bit-stream
- 2: **Initialization:**
- 3: Get  $\mathbf{y}, \mathbf{M}^q$  from the compressed bit-stream;
- 4: Set parameters  $\alpha, \beta, \mu$ ;
- 5: Set  $\mathbf{x}^{(0)} = \mathbf{y}, \mathbf{Z}_{G_k}^{(0)} = \mathbf{X}_{G_k}^{(0)}, k = 1, \dots, K$ ;
- 6: Calculate  $\sigma_e$  by Eq.(6);
- 7: Determine the feasible solution space  $\Omega$  by Eq. (16);
- 8: **For**  $t = 1, \dots, T$
- 9: Calculate  $\sigma_s^{(t-1)}$  by Eq. (36);
- 10: Compute  $\tau^{(t-1)} = \frac{(\sigma_s^{(t-1)})^2 \beta}{\alpha}$ ;
- 11: Construct  $\mathbf{X}_{G_k}^{(t-1)}$  for each exemplar patch by  $\mathbf{x}^{(t-1)}$ ;
- 12: Update all the  $\mathbf{Z}_{G_k}^{(t-1)}$  via **Algorithm 1**;
- 13: Compute  $\hat{\mathbf{x}}^{(t)}$  by Eq. (32);
- 14: Update  $\mathbf{x}^{(t)}$  by Eq. (33);
- 15: **End For**
- 16: **Output:** Final deblocking result  $\tilde{\mathbf{x}} = \mathbf{x}^{(T)}$

In particular, the setting of  $\sigma_e$  is adaptively determined by Eq. (6). For  $\sigma_s$ , since each  $\mathbf{Z}_{G_k}$  in Eq. (19) varies as the iteration number increases, its setting should be adaptively adjusted at each iteration. Here, the image  $\mathbf{z}_{t-1}$  that is reconstructed by all the  $\mathbf{Z}_{G_k}^{(t-1)}$  at  $(t-1)^{th}$  iteration is used to obtain robust  $\sigma_s^{(t-1)}$ .  $\mathbf{z}^{(t-1)}$  is formulated as

$$\mathbf{z}^{(t-1)} = \sum_{k=1}^K \mathbf{R}_{G_k}^T \mathbf{Z}_{G_k} \cdot / \sum_{k=1}^K \mathbf{R}_{G_k}^T \mathbf{1}_{G_k}, \quad (35)$$

where  $\cdot /$  stands for the element-wise division of two vectors and  $\mathbf{1}_{G_k}$  is a matrix of size  $B_s \times c$  with all the elements being 1.

After getting  $\mathbf{z}^{(t-1)}$ ,  $\sigma_s^{(t-1)}$  can be estimated by

$$\sigma_s^{(t-1)} = \delta \sqrt{\sigma_e^2 - \|\mathbf{z}^{(t-1)} - \mathbf{y}\|_2^2}, \quad (36)$$

where  $\delta$  is a scaling factor to control the variance estimation. Such technique has appeared in existing works, and please refer to [35] and [37] for further details. In this paper, we empirically set  $\delta$  to be 0.2, which has been verified suitable for all the QFs by extensive experiments.

### D. Summary

Up to now, the efficient solution for each separated minimization sub-problem has been acquired, and all the parameter settings are given. In light of all derivations above, a detailed descriptions of the proposed algorithm CONCOLOR for image deblocking are provided in **Algorithm 2**.

## V. EXPERIMENTAL RESULTS

In this section, extensive experimental results are presented to verify the performance of the proposed algorithm CONCOLOR for image deblocking. The default parameters are follows: the size of a data matrix is set to be  $36 \times 60$ , with  $B_s$  being 36 and  $c$  being 60. The width of overlapping between adjacent patches is 3 pixels. The range of training window for constructing the low-rank matrix, i.e.  $W_s \times W_s$  is set to be  $30 \times 30$ .  $\omega = 0.4, \mu = 10, \alpha = 10$ ,

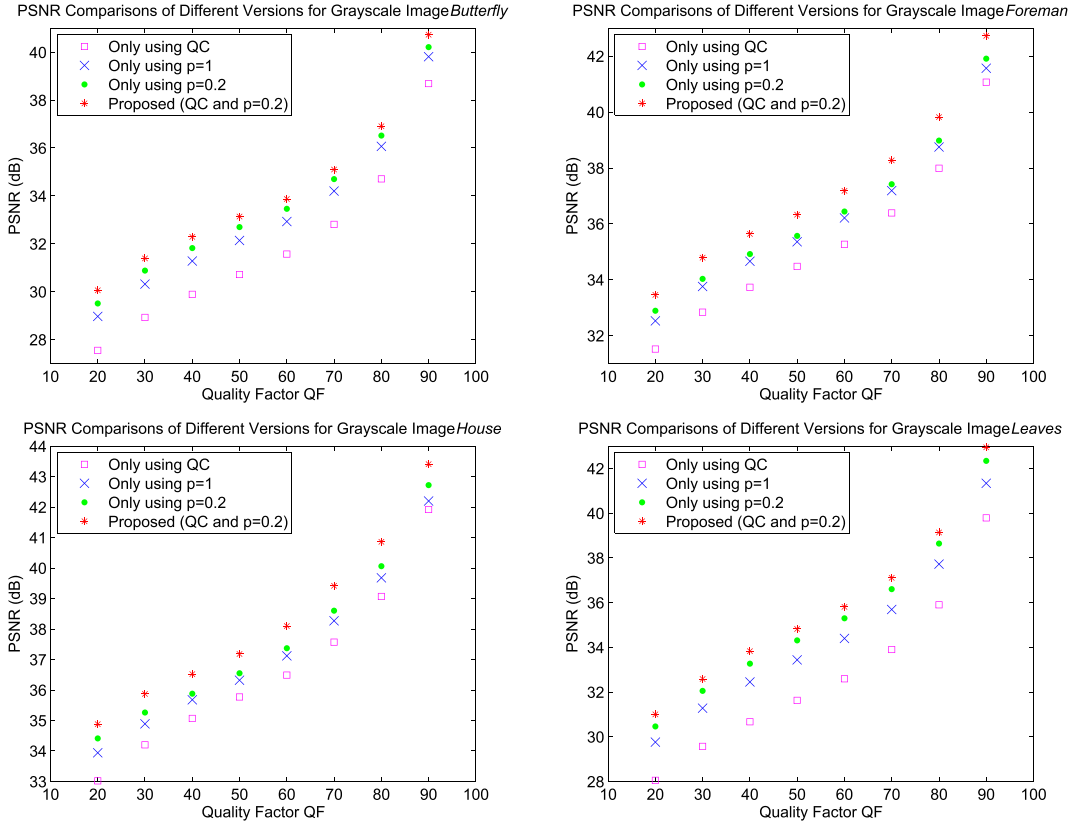


Fig. 6. PSNR result comparisons of different versions with various quality factors for four grayscale images: *Butterfly*, *House*, *Foreman* and *Leaves*.

$\beta = 200\sqrt{2c}$ ,  $T = 20$ . Without loss of generality,  $p$  in Eq. (9) is set to be 0.2. All the experiments are performed in Matlab 2013a on a Dell OPTIPLEX computer with Intel(R) Core(TM) i7 (2.80GHz), 8G memory, and Windows 7 operating system. The source code of CONCOLOR and all the experimental results can be downloaded from the following website <http://idm.pku.edu.cn/staff/zhangjian/CONCOLOR/>.

#### A. Effectiveness of Non-Convex Low-Rank Prior and Quantization Constraint Prior

In order to demonstrate the effectiveness of each component and the combination of the proposed CONCOLOR such as quantization constraint (QC) and low-rank prior, we first implement four variants of the proposed deblocking algorithm: a) Only using QC, b) Only using  $p = 1$ , c) Only using  $p = 0.2$ , and d) Proposed (QC and  $p = 0.2$ ). We conduct experiments on four grayscale images with various JPEG quality factors from 20 to 90. The PSNR result comparisons of different versions are illustrated in Fig. 6, where ‘□’, ‘×’, ‘•’ and ‘\*’ denote the versions of Only using QC, Only using  $p = 1$ , Only using  $p = 0.2$ , and Proposed (QC and  $p = 0.2$ ), respectively. From Fig. 6, it is clear to show the evidence of each claim of novel of the proposed algorithm. Obviously, the version of Only using QC produces the worst results. One can observe that the version of Only using  $p = 0.2$  performs better than the version of Only using  $p = 1$ . The proposed deblocking algorithm CONCOLOR combining QC and  $p = 0.2$  achieves the best

highest PSNR results among all the versions over all the cases, further demonstrating its effectiveness.

#### B. Comparison With State-of-the-Art Algorithms

The proposed CONCOLOR is compared with five representative image deblocking methods, i.e. Sun’s [26], Foi’s [8], DicTV [23], Zhang’s [28], Ren’s [33], and two representative image denoising methods, i.e. BM3D [46] and WNNM [37]. The results of all the competing algorithms are generated by the original authors softwares with the optimal parameters. It is worth emphasizing that Ren’s [33] and WNNM [37] both exploit low-rank prior via the nuclear norm, and they generate the state-of-the-art image deblocking and denoising results, respectively.

For comparison, all the standard test images shown in Fig. 7 are first encoded by a JPEG coder [1] with different quality factors (QF) that correspond to different quantization matrices, and then decoded using the standard JPEG decoder followed by different image deblocking methods. To evaluate the quality of the deblocking image, in addition to PSNR and the well-known perceptual quality metric SSIM [47], a block-sensitive index, named PSNR-B [48], which is specially designed to assess blocky and deblocked images, is also adopted.

The PSNR, SSIM and PSNR-B result comparisons for all grayscale test images in the cases of  $QF = 5$  and  $QF = 10$  are provided in Table I, Table II and Table III, respectively, with the best results highlighted in bold. The proposed CONCOLOR achieves the highest PSNR, SSIM and



Fig. 7. All test images including nine standard grayscale images and five standard color images. From top to bottom and left to right: *Barbara, Butterfly, Cameraman, Foreman, House, Leaves, Lena, Parrots, Peppers, Butterfly, Foreman, Barbara, House and Leaves.*

TABLE I  
PSNR (UNIT: dB) RESULTS OF ALL COMPETITIVE ALGORITHMS FOR GRAYSCALE IMAGE DEBLOCKING

Test image	Barbara	Butterfly	Camera.	Forem.	House	Leaves	Lena	Parrots	Peppers	Average
Size	256×256	256×256	256×256	288×352	256×256	256×256	512×512	256×256	512×512	PSNR
Quality Factor = 5										
JPEG	23.86	22.58	24.45	26.28	27.77	22.49	27.33	26.19	27.17	25.35
Sun's [26]	24.78	23.83	25.25	27.64	29.09	23.47	28.87	27.45	29.05	26.60
Foi's [8]	25.00	24.69	25.53	28.09	29.30	24.28	28.95	27.61	29.04	26.94
Zhang's [28]	25.23	24.20	25.39	28.03	29.24	24.13	29.00	27.78	29.07	26.90
Ren's [33]	25.33	24.58	25.46	28.39	29.66	24.56	29.07	27.87	29.07	27.11
BM3D [46]	24.96	24.05	25.27	27.85	29.21	24.02	28.63	27.33	28.52	26.65
DicTV [23]	24.35	23.10	24.54	27.04	28.45	23.01	28.07	26.83	27.95	25.93
WNNM [37]	25.22	24.75	25.49	28.33	29.62	24.68	28.95	27.80	28.99	27.09
Proposed	<b>25.70</b>	<b>25.30</b>	<b>25.61</b>	<b>29.08</b>	<b>30.12</b>	<b>24.99</b>	<b>29.51</b>	<b>28.27</b>	<b>29.61</b>	<b>27.58</b>
Quality Factor = 10										
JPEG	26.29	25.24	26.47	29.11	30.56	25.40	30.41	28.96	30.14	28.06
Sun's [26]	27.10	26.52	27.26	30.31	32.00	26.60	31.72	30.04	31.62	29.24
Foi's [8]	27.36	27.25	27.48	30.94	32.09	27.30	31.84	30.15	31.69	29.57
Zhang's [28]	27.77	26.83	27.45	30.78	32.11	27.26	31.92	30.50	31.68	29.59
Ren's [33]	27.86	27.17	27.43	30.94	32.41	27.59	31.92	30.34	31.63	29.70
BM3D [46]	27.52	26.64	27.25	30.72	32.07	26.98	31.77	30.05	31.42	29.38
DicTV [23]	27.07	26.09	26.92	30.30	31.77	26.33	31.55	29.82	31.29	29.01
WNNM [37]	27.81	27.22	27.40	30.94	32.42	27.66	31.93	30.33	31.64	29.71
Proposed	<b>28.50</b>	<b>27.90</b>	<b>27.72</b>	<b>31.46</b>	<b>33.04</b>	<b>28.20</b>	<b>32.19</b>	<b>30.66</b>	<b>31.94</b>	<b>30.18</b>

TABLE II  
SSIM RESULTS OF ALL COMPETITIVE ALGORITHMS FOR GRAYSCALE IMAGE DEBLOCKING

Test image	Barbara	Butterfly	Camera.	Forem.	House	Leaves	Lena	Parrots	Peppers	Average
Size	256×256	256×256	256×256	288×352	256×256	256×256	512×512	256×256	512×512	SSIM
Quality Factor = 5										
JPEG	0.6563	0.7378	0.7283	0.7307	0.7733	0.7775	0.7367	0.7581	0.7078	0.7341
Sun's [26]	0.7100	0.8231	0.7687	0.8106	0.8113	0.8380	0.8061	0.8323	0.7931	0.7993
Foi's [8]	0.7121	0.8472	0.7705	0.8197	0.8142	0.8651	0.8037	0.8302	0.7902	0.8059
Zhang's [28]	0.7132	0.8313	0.7672	0.8171	0.8141	0.8548	0.8035	0.8308	0.7895	0.8024
Ren's [33]	0.7123	0.8419	0.7666	0.8217	0.8197	0.8720	0.8010	0.8310	0.7876	0.8060
BM3D [46]	0.7068	0.8184	0.7607	0.8004	0.8082	0.8510	0.7837	0.8118	0.7639	0.7895
DicTV [23]	0.6932	0.7769	0.6658	0.7785	0.7963	0.8104	0.7744	0.8005	0.7456	0.7602
WNNM [37]	0.7105	0.8445	0.7674	0.8184	0.8178	0.8749	0.7947	0.8287	0.7827	0.8044
Proposed	<b>0.7357</b>	<b>0.8667</b>	<b>0.7666</b>	<b>0.8377</b>	<b>0.8285</b>	<b>0.8882</b>	<b>0.8169</b>	<b>0.8460</b>	<b>0.8031</b>	<b>0.8210</b>
Quality Factor = 10										
JPEG	0.7901	0.8235	0.7965	0.8084	0.8183	0.8609	0.8183	0.8336	0.7839	0.8148
Sun's [26]	0.8205	0.8871	0.8358	0.8596	0.8504	0.9138	0.8590	0.8783	0.8322	0.8596
Foi's [8]	0.8297	0.9014	0.8333	0.8653	0.8491	0.9282	0.8586	0.8778	0.8318	0.8639
Zhang's [28]	0.8288	0.8923	0.8329	0.8654	0.8513	0.9212	0.8597	0.8804	0.8317	0.8626
Ren's [33]	0.8359	0.9010	0.8259	0.8658	0.8526	0.9309	0.8571	0.8775	0.8300	0.8641
BM3D [46]	0.8338	0.8896	0.8240	0.8623	0.8492	0.9207	0.8549	0.8749	0.8250	0.8594
DicTV [23]	0.8262	0.8699	0.8046	0.8573	0.8484	0.9032	0.8559	0.8741	0.8244	0.8515
WNNM [37]	0.8362	0.9019	0.8248	0.8663	0.8531	0.9325	0.8571	0.8775	0.8303	0.8644
Proposed	<b>0.8524</b>	<b>0.9142</b>	<b>0.8401</b>	<b>0.8746</b>	<b>0.8609</b>	<b>0.9406</b>	<b>0.8661</b>	<b>0.8842</b>	<b>0.8358</b>	<b>0.8743</b>

PSNR-B among the eight comparative algorithms over all the cases with significant gain over previous works. Concretely, it is obvious to see that Sun's and BM3D performs better

than DicTV, and Foi's and Zhang's produce better results than Sun's and BM3D. Ren's and WNNM show very similar performance, which are superior to Foi's and Zhang's. As for

TABLE III  
PSNR-B (UNIT: dB) RESULTS OF ALL COMPETITIVE ALGORITHMS FOR GRAYSCALE IMAGE DEBLOCKING

Test image	Barbara	Butterfly	Camera.	Forem.	House	Leaves	Lena	Parrots	Peppers	Average
Size	256×256	256×256	256×256	288×352	256×256	256×256	512×512	256×256	512×512	<b>PSNR-B</b>
Quality Factor = 5										
JPEG	21.10	19.17	21.89	23.61	24.57	18.87	24.49	23.23	24.67	22.40
Sun's [26]	23.73	22.17	23.97	27.38	27.86	22.06	28.18	26.14	28.62	25.57
Foi's [8]	24.45	22.97	24.46	28.09	28.41	22.70	28.55	26.58	28.93	26.13
Zhang's [28]	24.83	23.35	24.75	28.03	28.11	23.32	28.42	27.32	28.70	26.32
Ren's [33]	25.10	23.99	25.01	28.39	28.83	23.88	28.82	27.61	29.07	26.75
BM3D [46]	24.11	22.56	24.13	27.75	27.66	22.43	27.67	26.21	27.90	25.60
DicTV [23]	22.45	20.25	22.67	25.53	26.08	19.99	26.23	24.83	26.58	23.84
WNNM [37]	24.84	23.81	24.76	28.33	28.58	23.85	28.50	27.35	28.91	26.55
Proposed	<b>25.70</b>	<b>25.14</b>	<b>25.39</b>	<b>29.08</b>	<b>29.55</b>	<b>24.83</b>	<b>29.39</b>	<b>28.27</b>	<b>29.61</b>	<b>27.44</b>
Quality Factor = 10										
JPEG	22.96	21.81	23.65	26.46	27.25	21.47	27.30	25.91	27.76	24.95
Sun's [26]	25.53	24.64	25.48	30.04	30.61	24.50	30.77	28.57	31.43	27.95
Foi's [8]	25.89	24.75	25.69	30.93	30.69	24.49	31.02	28.64	31.56	28.18
Zhang's [28]	27.31	26.12	26.62	30.78	30.70	26.33	31.3	30.1	31.64	28.99
Ren's [33]	26.75	25.92	26.23	30.94	31.1	26.02	31.43	29.70	31.63	28.86
BM3D [46]	25.87	24.90	25.61	30.72	30.37	24.80	30.73	28.78	31.21	28.11
DicTV [23]	24.86	23.59	24.92	29.47	29.71	23.41	30.10	28.10	30.68	27.20
WNNM [37]	26.69	25.89	26.11	30.94	31.01	26.16	31.39	29.66	31.64	28.83
Proposed	<b>28.16</b>	<b>27.80</b>	<b>27.27</b>	<b>31.46</b>	<b>32.18</b>	<b>27.98</b>	<b>32.08</b>	<b>30.66</b>	<b>31.94</b>	<b>29.95</b>



Fig. 8. Visual quality comparison of image deblocking for grayscale image *Foreman* in the case of QF = 5. From left to right and top to bottom: original image, JPEG compressed image (PSNR = 26.28 dB; SSIM = 0.7307; PSNR-B = 23.61 dB), the deblocking results by Sun's (PSNR = 27.64 dB; SSIM = 0.8106; PSNR-B = 27.38 dB), Foi's (PSNR = 28.09 dB; SSIM = 0.8197; PSNR-B = 28.09 dB), Zhang's (PSNR = 28.03 dB; SSIM = 0.8171; PSNR-B = 28.03 dB), Ren's (PSNR = 28.39 dB; SSIM = 0.8217; PSNR-B = 28.39 dB), BM3D (PSNR = 27.85 dB; SSIM = 0.8004; PSNR-B = 27.75 dB), DicTV (PSNR = 27.04 dB; SSIM = 0.7785; PSNR-B = 25.53 dB), WNNM (PSNR = 28.33 dB; SSIM = 0.8184; PSNR-B = 28.33 dB) and the proposed CONCOLOR (PSNR = **29.08** dB; SSIM = **0.8377**; PSNR-B = **29.08** dB).

CONCOLOR, in the case of QF = 5, it achieves (0.47 dB, 0.49 dB) gains in PSNR, (0.0150, 0.0166) gains in SSIM and (0.69 dB, 0.89 dB) gains in PSNR-B over Ren's and WNNM on average; in the case of QF = 10, it achieves (0.48 dB, 0.47 dB) gains in PSNR, (0.0102, 0.0099) gains in SSIM and (1.09 dB, 1.11 dB) gains in PSNR-B over Ren's and WNNM on average. In particular, in the case of QF = 5 for image *Foreman*, CONCOLOR achieves up to (1.44 dB, 0.99 dB, 1.05 dB, 0.69 dB, 1.23 dB, 2.04 dB, 0.75 dB) PSNR gains and (1.70 dB, 0.99 dB, 1.05 dB, 0.69 dB, 1.23 dB, 3.55 dB, 0.75 dB) PSNR-B gains over Sun's, Foi's, Zhang's, Ren's, BM3D, DicTV, and WNNM, respectively. The visual quality comparisons in the cases of QF = 5 and QF = 10 for two grayscale test images are provided in Fig. 8 and Fig. 9. One can see that the blocking artifacts are obvious in the images

decoded directly by the standard JPEG. DicTV, Sun's and BM3D can suppress the blocking artifacts partially, but many blocking artifacts are still visible in reconstructed images. Foi's and Zhang's usually generate better results than Sun's and BM3D. However, they often produce noticeable zigzag artifacts and blur effects along image edges. Ren's and WNNM are good at capturing image edges, but it may produce ghost effects and generate some incorrect textures. The proposed CONCOLOR not only reduces most of the blocking artifacts significantly, but also provides better reconstruction on both edges and textures than other competing methods.

Furthermore, we extend the proposed CONCOLOR from grayscale images to color images. Since the JPEG standard compresses color images in the YUV color space, it is natural to first decompose the JPEG-compressed color image into



Fig. 9. Visual quality comparison of image deblocking for grayscale image *Barbara* in the case of QF = 10. From left to right and top to bottom: original image, JPEG compressed image (PSNR = 26.29 dB; SSIM = 0.7901; PSNR-B = 22.96 dB), the deblocking results by Sun's (PSNR = 27.10 dB; SSIM = 0.8205; PSNR-B = 25.53 dB), Foi's (PSNR = 27.36 dB; SSIM = 0.8297; PSNR-B = 25.89 dB), Zhang's (PSNR = 27.77 dB; SSIM = 0.8288; PSNR-B = 27.31 dB), Ren's (PSNR = 27.86 dB; SSIM = 0.8359; PSNR-B = 26.75 dB), BM3D (PSNR = 27.52 dB; SSIM = 0.8338; PSNR-B = 25.87 dB), DicTV (PSNR = 27.07 dB; SSIM = 0.8262; PSNR-B = 24.86 dB), WNNM (PSNR = 27.81 dB; SSIM = 0.8362; PSNR-B = 26.69 dB) and the proposed CONCOLOR (PSNR = **28.50** dB; SSIM = **0.8524**; PSNR-B = **28.16** dB).

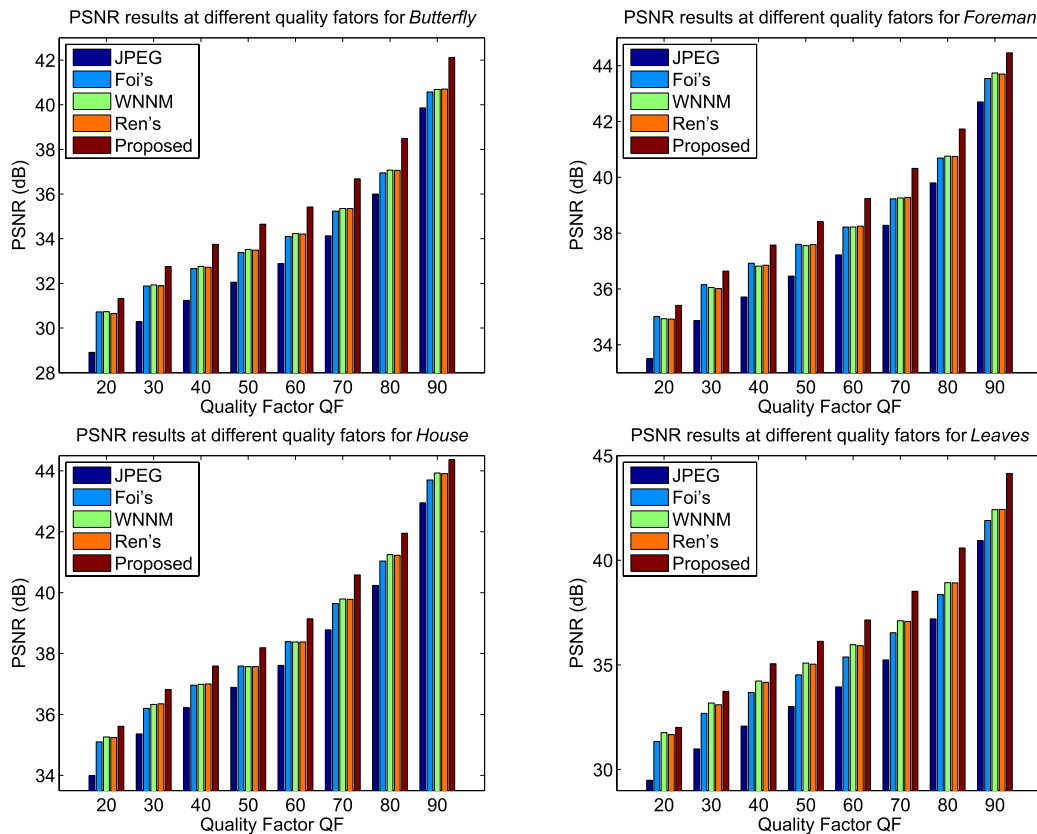


Fig. 10. Comparisons of PSNR results at different quality factors in the range [20 90] for four color test images: *Barbara*, *Butterfly*, *Foreman*, *House*, and *Leaves*.

one luminance channels and two chrominance channels, and then apply our proposed CONCOLOR in the resulting three channels, respectively. In particular, the noise variance of each component channel is calculated by Eq. (6) from the corresponding quantization table, and the proposed deblocking algorithm as described in **Algorithm 2** is invoked to deal with

each component channel, separately. Extensive experiments with various JPEG quality factors from 20 to 90 are conducted on five color test images shown in Fig. 7. Fig. 10 presents the reconstruction PSNR comparisons among JPEG, Foi's, WNNM, Ren's, and the proposed CONCOLOR. As the human eyes are sensitive to the luminance and insensitive to

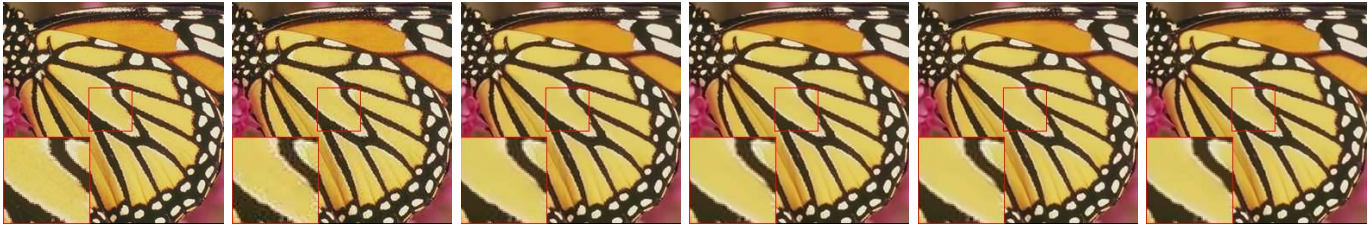


Fig. 11. Visual quality comparison of image deblocking for color image *Butterfly* in the case of  $QF = 40$ . From left to right: original image, JPEG compressed image (PSNR = 31.24 dB), the deblocking results by Foi's (PSNR = 32.66 dB), WNNM (PSNR = 32.76 dB), Ren's (PSNR = 32.72 dB) and the proposed CONCOLOR (PSNR = 33.75 dB).

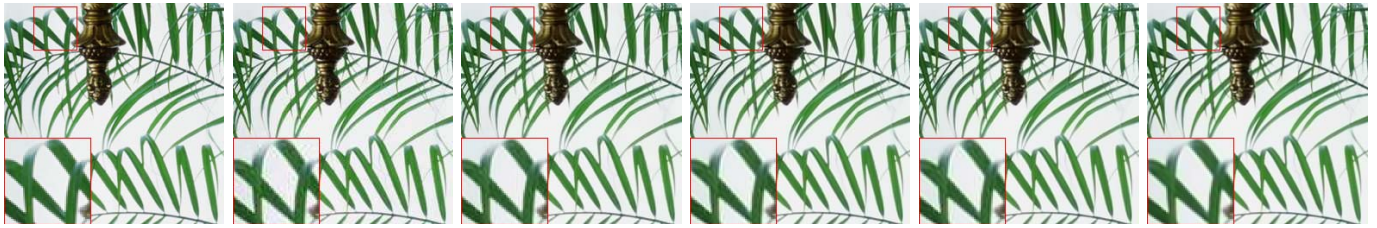


Fig. 12. Visual quality comparison of image deblocking for color image *Leaves* in the case of  $QF = 50$ . From left to right: original image, JPEG compressed image (PSNR = 33.01 dB), the deblocking results by Foi's (PSNR = 34.53 dB), WNNM (PSNR = 35.09 dB), Ren's (PSNR = 35.04 dB) and the proposed CONCOLOR (PSNR = 36.13 dB).

the colors, we only use the luminance component to compute PSNR in the experiments of color images.

From Fig. 10, it is also obvious to see that CONCOLOR works well over a wide quality (or bit rate) range, and outperforms current state-of-the-art algorithms Ren's and WNNM over all the cases. Especially, for color image *Butterfly*, the proposed CONCOLOR obtains on average 2.48 dB, 1.21 dB, 1.11 dB and 1.14 dB PSNR gains over JPEG, Foi's, WNNM and Ren's; for color image *Foreman*, the proposed CONCOLOR obtains on average 1.91 dB, 0.80 dB, 0.81 dB and 0.80 dB PSNR gains over JPEG, Foi's, WNNM and Ren's; for color image *Leaves*, the proposed CONCOLOR obtains on average 3.06 dB, 1.62 dB, 1.08 dB and 1.13 dB PSNR gains over JPEG, Foi's, WNNM and Ren's. Fig. 11 and Fig. 12 further show visual quality comparisons in the cases of  $QF = 40$  for color image *Butterfly* and  $QF = 50$  for color image *Leaves*. The proposed CONCOLOR not only reduces most of the blocking artifacts significantly, but also provides better reconstruction on both edges and textures than other competing methods, which fully demonstrates the effectiveness of CONCOLOR.

### C. Effect of Quantization Constraint Parameter

This subsection gives some descriptions about how sensitive the performance is affected by the quantization constraint parameter  $\omega$ . In this paper, we adopt narrow quantization constraint (NQC) by setting  $\omega = 0.4$  rather than traditional  $\omega = 0.5$ . Table IV presents the performance comparisons with various  $\omega$  for three grayscale test images. Obviously, the setting of  $\omega = 0.4$  achieves better results than that of  $\omega = 0.5$ , obtaining about 0.2 dB gain on average, which further verify the effectiveness of NQC.

### D. Algorithm Complexity and Computational Time

Now let's now discuss about the complexity and computational time of the proposed algorithm CONCOLOR.

TABLE IV  
PSNR (dB) COMPARISONS WITH VARIOUS  $\omega$

Test Setting		<i>Barbara</i>	<i>Butterfly</i>	<i>House</i>	Avg.
QF=5	$\omega = 0.5$	25.61	25.08	29.93	26.87
	$\omega = 0.4$	25.70	25.30	30.12	<b>27.04</b>
QF=10	$\omega = 0.5$	28.29	27.64	32.76	29.56
	$\omega = 0.4$	28.50	27.90	33.04	<b>29.81</b>

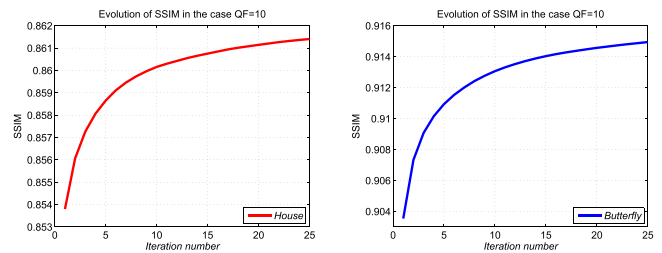


Fig. 13. SSIM evolutions achieved by proposed CONCOLOR versus iteration numbers for two grayscale images: *House* (Left) and *Butterfly* (Right).

It is apparent that the complexity of CONCOLOR mainly lies in the non-convex low-rank minimization sub-problem in Sec. IV.A. Assume that the number of image pixels is  $N^2$ , and that the average time to find similar patches for each exemplar patch is  $T_f$ . Due to that the SVD operation of each matrix with size of  $B_s \times c$  is  $\mathcal{O}(B_s c^2)$ , the total complexity of CONCOLOR is hence  $\mathcal{O}(N^2 (B_s c^2 + T_f))$ . As illustrated in Fig. 13, the proposed CONCOLOR converges after twenty iterations, and that's just the reason we set  $T = 20$ . In particular, as for a  $256 \times 256$  grayscale image, the proposed CONCOLOR requires about 7~8 minutes for image deblocking on an Intel(R) Core(TM) i7 2.80GHz PC under Matlab R2013a environment. On going work utilizes GPU hardware to address the parallelization for accelerating

TABLE V  
COMPUTATIONAL TIME COMPARISONS OF DIFFERENT METHODS FOR A  $256 \times 256$  GRAYSCALE IMAGE (UNIT: s)

Sun's [26]	Foi's [8]	Zhang's [28]	Ren's [33]	BM3D [46]	DicTV [23]	WNNM [37]	Proposed
132	6.1	251	36	3.4	53	230	442

the proposed algorithm. All computational time comparisons of different methods to deal with a  $256 \times 256$  grayscale image are shown in Table V.

## VI. CONCLUSION

In this paper, in order to reduce blocking artifacts and obtain high-quality image, a novel image deblocking algorithm is proposed by utilizing CONstrained Non-CONvex LOw-Rank (CONCOLOR) model under maximum a posteriori framework. The  $l_p$  ( $0 < p < 1$ ) penalty function is extended on singular values of a matrix to characterize low-rank prior model rather than the nuclear norm, while the quantization constraint is explicitly transformed into the feasible solution space to constrain the non-convex low-rank optimization. To make the proposed optimization problem tractable, an alternatively minimizing strategy with adaptive parameter adjustment is developed. It is worth emphasizing that the proposed algorithm CONCOLOR outperforms current state-of-the-art algorithms in both PSNR and visual perception. Future work includes the direct extensions of CONCOLOR on video deblocking applications.

## ACKNOWLEDGMENT

The authors would like to thank Prof. Lei Zhang for his efforts in coordinating the review of the manuscript, and also would like to thank the anonymous reviewers for their constructive suggestions to improve the manuscript.

## REFERENCES

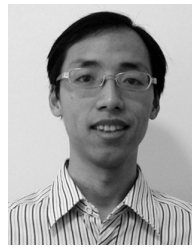
- [1] G. K. Wallace, "The JPEG still picture compression standard," *Commun. ACM*, vol. 34, no. 4, pp. 30–44, 1991.
- [2] T. Wiegand, G. J. Sullivan, G. Bjøntegaard, and A. Luthra, "Overview of the H.264/AVC video coding standard," *IEEE Trans. Circuits Syst. Video Technol.*, vol. 13, no. 7, pp. 560–576, Jul. 2003.
- [3] G. J. Sullivan, J.-R. Ohm, W.-J. Han, and T. Wiegand, "Overview of the high efficiency video coding (HEVC) standard," *IEEE Trans. Circuits Syst. Video Technol.*, vol. 22, no. 12, pp. 1649–1668, Dec. 2012.
- [4] M.-Y. Shen and C.-C. J. Kuo, "Review of postprocessing techniques for compression artifact removal," *J. Vis. Commun. Image Represent.*, vol. 9, no. 1, pp. 2–14, 1998.
- [5] C.-H. Yeh, L.-W. Kang, Y.-W. Chiou, C.-W. Lin, and S.-J. F. Jiang, "Self-learning-based post-processing for image/video deblocking via sparse representation," *J. Vis. Commun. Image Represent.*, vol. 25, no. 5, pp. 891–903, 2014.
- [6] G. Zhai, W. Zhang, X. Yang, W. Lin, and Y. Xu, "Efficient image deblocking based on postfiltering in shifted windows," *IEEE Trans. Circuits Syst. Video Technol.*, vol. 18, no. 1, pp. 122–126, Jan. 2008.
- [7] G. Zhai, W. Zhang, X. Yang, W. Lin, and Y. Xu, "Efficient deblocking with coefficient regularization, shape-adaptive filtering, and quantization constraint," *IEEE Trans. Multimedia*, vol. 10, no. 5, pp. 735–745, Aug. 2008.
- [8] A. Foi, V. Katkovnik, and K. Egiazarian, "Pointwise shape-adaptive DCT for high-quality denoising and deblocking of grayscale and color images," *IEEE Trans. Image Process.*, vol. 16, no. 5, pp. 1395–1411, May 2007.
- [9] R. Zhang, W. Ouyang, and W.-K. Cham, "Image postprocessing by non-local Kuan's filter," *J. Vis. Commun. Image Represent.*, vol. 22, no. 3, pp. 251–262, 2011.
- [10] N. C. Francisco, N. M. M. Rodrigues, E. A. B. da Silva, and S. M. M. de Faria, "A generic post-deblocking filter for block based image compression algorithms," *Signal Process., Image Commun.*, vol. 27, no. 9, pp. 985–997, 2012.
- [11] C. Wang, J. Zhou, and S. Liu, "Adaptive non-local means filter for image deblocking," *Signal Process., Image Commun.*, vol. 28, no. 5, pp. 522–530, 2013.
- [12] G. Farinella and S. Battiato, "On the application of structured sparse model selection to JPEG compressed images," in *Proc. 3rd Int. Workshop Comput. Color Imag.*, Milan, Italy, Apr. 2011, pp. 137–151.
- [13] J. Kim, "Adaptive blocking artifact reduction using wavelet-based block analysis," *IEEE Trans. Consum. Electron.*, vol. 55, no. 2, pp. 933–940, May 2009.
- [14] S. B. Yoo, K. Choi, and J. B. Ra, "Post-processing for blocking artifact reduction based on inter-block correlation," *IEEE Trans. Multimedia*, vol. 16, no. 6, pp. 1536–1548, Oct. 2014.
- [15] J. Zhang, S. Ma, Y. Zhang, and W. Gao, "Image deblocking using group-based sparse representation and quantization constraint prior," in *Proc. IEEE Int. Conf. Image Process.*, Sep. 2015, pp. 306–310.
- [16] A. Zakhori, "Iterative procedures for reduction of blocking effects in transform image coding," *IEEE Trans. Circuits Syst. Video Technol.*, vol. 2, no. 1, pp. 91–95, Mar. 1992.
- [17] Y. Yang, N. P. Galatsanos, and A. K. Katsaggelos, "Projection-based spatially adaptive reconstruction of block-transform compressed images," *IEEE Trans. Image Process.*, vol. 4, no. 7, pp. 896–908, Jul. 1995.
- [18] Y. Yang and N. P. Galatsanos, "Removal of compression artifacts using projections onto convex sets and line process modeling," *IEEE Trans. Image Process.*, vol. 6, no. 10, pp. 1345–1357, Oct. 1997.
- [19] S. H. Park and D. S. Kim, "Theory of projection onto the narrow quantization constraint set and its application," *IEEE Trans. Image Process.*, vol. 8, no. 10, pp. 1361–1373, Oct. 1999.
- [20] K. Bredies and M. Holler, "A total variation-based JPEG decompression model," *SIAM J. Imag. Sci.*, vol. 5, no. 1, pp. 366–393, 2012.
- [21] C. Jung, L. Jiao, H. Qi, and T. Sun, "Image deblocking via sparse representation," *Signal Process., Image Commun.*, vol. 27, no. 6, pp. 663–677, 2012.
- [22] X. Liu, X. Wu, and D. Zhao, "Sparsity-based soft decoding of compressed images in transform domain," in *Proc. IEEE Int. Conf. Image Process.*, Sep. 2013, pp. 563–566.
- [23] H. Chang, M. K. Ng, and T. Zeng, "Reducing artifacts in JPEG decompression via a learned dictionary," *IEEE Trans. Signal Process.*, vol. 62, no. 3, pp. 718–728, Feb. 2014.
- [24] T. P. O'Rourke and R. L. Stevenson, "Improved image decompression for reduced transform coding artifacts," *IEEE Trans. Circuits Syst. Video Technol.*, vol. 5, no. 6, pp. 490–499, Dec. 1995.
- [25] T. Meier, K. N. Ngan, and G. Crebbin, "Reduction of blocking artifacts in image and video coding," *IEEE Trans. Circuits Syst. Video Technol.*, vol. 9, no. 3, pp. 490–500, Apr. 1999.
- [26] D. Sun and W.-K. Cham, "Postprocessing of low bit-rate block DCT coded images based on a fields of experts prior," *IEEE Trans. Image Process.*, vol. 16, no. 11, pp. 2743–2751, Nov. 2007.
- [27] X. Zhang, R. Xiong, S. Ma, and W. Gao, "Reducing blocking artifacts in compressed images via transform-domain non-local coefficients estimation," in *Proc. IEEE Int. Conf. Multimedia Expo*, Jul. 2012, pp. 836–841.
- [28] X. Zhang, R. Xiong, X. Fan, S. Ma, and W. Gao, "Compression artifact reduction by overlapped-block transform coefficient estimation with block similarity," *IEEE Trans. Image Process.*, vol. 22, no. 12, pp. 4613–4626, Dec. 2013.
- [29] J. Zhang, R. Xiong, S. Ma, and D. Zhao, "High-quality image restoration from partial random samples in spatial domain," in *Proc. IEEE Int. Conf. Vis. Commun. Image Process.*, Nov. 2011, pp. 1–4.
- [30] J. Zhang, D. Zhao, C. Zhao, R. Xiong, S. Ma, and W. Gao, "Image compressive sensing recovery via collaborative sparsity," *IEEE J. Emerg. Sel. Topics Circuits Syst.*, vol. 2, no. 3, pp. 380–391, Sep. 2012.
- [31] J. Zhang, R. Xiong, C. Zhao, S. Ma, and D. Zhao, "Exploiting image local and nonlocal consistency for mixed Gaussian-impulse noise removal," in *Proc. IEEE Int. Conf. Multimedia Expo*, Jul. 2012, pp. 592–597.

- [32] H. Liu, R. Xiong, J. Zhang, and W. Gao, "Image denoising via adaptive soft-thresholding based on non-local samples," in *Proc. IEEE Int. Conf. Comput. Vis. Pattern Recognit.*, Jun. 2015, pp. 484–492.
- [33] J. Ren, J. Liu, M. Li, W. Bai, and Z. Guo, "Image blocking artifacts reduction via patch clustering and low-rank minimization," in *Proc. IEEE Data Commun. Conf. (DCC)*, Mar. 2013, p. 516.
- [34] M. Li, J. Liu, J. Ren, and Z. Guo, "Patch-based image deblocking using geodesic distance weighted low-rank approximation," in *Proc. IEEE Int. Conf. Vis. Commun. Image Process.*, Dec. 2014, pp. 101–104.
- [35] W. Dong, G. Shi, and X. Li, "Nonlocal image restoration with bilateral variance estimation: A low-rank approach," *IEEE Trans. Image Process.*, vol. 22, no. 2, pp. 700–711, Feb. 2013.
- [36] H. Ji, S. Huang, Z. Shen, and Y. Xu, "Robust video restoration by joint sparse and low rank matrix approximation," *SIAM J. Imag. Sci.*, vol. 4, no. 4, pp. 1122–1142, 2011.
- [37] S. Gu, L. Zhang, W. Zuo, and X. Feng, "Weighted nuclear norm minimization with application to image denoising," in *Proc. IEEE Int. Conf. Comput. Vis. Pattern Recognit.*, Jun. 2014, pp. 2862–2869.
- [38] E. J. Candès, X. Li, Y. Ma, and J. Wright, "Robust principal component analysis?" *J. ACM*, vol. 58, no. 3, pp. 11:1–11:37, May 2011.
- [39] J.-F. Cai, E. J. Candès, and Z. Shen, "A singular value thresholding algorithm for matrix completion," *SIAM J. Optim.*, vol. 20, no. 4, pp. 1956–1982, 2010.
- [40] B. K. Gunturk, Y. Altunbasak, and R. M. Mersereau, "Super-resolution reconstruction of compressed video using transform-domain statistics," *IEEE Trans. Image Process.*, vol. 13, no. 1, pp. 33–43, Jan. 2004.
- [41] M. A. Robertson and R. L. Stevenson, "DCT quantization noise in compressed images," *IEEE Trans. Circuits Syst. Video Technol.*, vol. 15, no. 1, pp. 27–38, Jan. 2005.
- [42] J. Zhang, D. Zhao, R. Xiong, S. Ma, and W. Gao, "Image restoration using joint statistical modeling in a space-transform domain," *IEEE Trans. Circuits Syst. Video Technol.*, vol. 24, no. 6, pp. 915–928, Jun. 2014.
- [43] J. Zhang, D. Zhao, and W. Gao, "Group-based sparse representation for image restoration," *IEEE Trans. Image Process.*, vol. 23, no. 8, pp. 3336–3351, Aug. 2014.
- [44] C. Lu, J. Tang, S. Yan, and Z. Lin, "Generalized nonconvex nonsmooth low-rank minimization," in *Proc. IEEE Int. Conf. Comput. Vis. Pattern Recognit.*, Jun. 2014, pp. 4130–4137.
- [45] K. Chen, H. Dong, and K.-S. Chan, "Reduced rank regression via adaptive nuclear norm penalization," *Biometrika*, vol. 100, no. 4, pp. 901–920, 2012.
- [46] K. Dabov, A. Foi, V. Katkovnik, and K. Egiazarian, "Image denoising by sparse 3-D transform-domain collaborative filtering," *IEEE Trans. Image Process.*, vol. 16, no. 8, pp. 2080–2095, Aug. 2007.
- [47] Z. Wang, A. C. Bovik, H. R. Sheikh, and E. P. Simoncelli, "Image quality assessment: From error visibility to structural similarity," *IEEE Trans. Image Process.*, vol. 13, no. 4, pp. 600–612, Apr. 2004.
- [48] C. Yim and A. C. Bovik, "Quality assessment of deblocked images," *IEEE Trans. Image Process.*, vol. 20, no. 1, pp. 88–98, Jan. 2011.



**Jian Zhang** (M'14) received the B.S. degree from the Department of Mathematics, Harbin Institute of Technology (HIT), Harbin, China, in 2007, and the M.Eng. and Ph.D. degrees from the School of Computer Science and Technology, HIT, in 2009 and 2014, respectively. He is currently a Post-Doctoral Fellow with the Institute of Digital Media, Peking University, Beijing, China. His research interests include image/video compression and restoration, compressive sensing, sparse representation, and dictionary learning. He was a recipient of the best paper

award and the Best Student Paper Award at the IEEE International Conference on Visual Communication and Image Processing in 2011 and 2015, respectively.



**Ruiqin Xiong** (M'08) received the B.S. degree from the University of Science and Technology of China, Hefei, China, in 2001, and the Ph.D. degree from the Institute of Computing Technology, Chinese Academy of Sciences, Beijing, China, in 2007.

He was a Research Intern with Microsoft Research Asia from 2002 to 2007 and a Senior Research Associate with the University of New South Wales, Australia, from 2007 to 2009. He joined the School of Electronic Engineering and Computer Science, Peking University, as a Research Professor, in 2010.

He has published over 80 technical papers in referred international journals and conference proceedings. His research interests include statistical image modeling, image and video processing, video compression, and multimedia communication.



**Chen Zhao** received the B.S. degree from the School of Software Engineering, Sichuan University, Chengdu, China, in 2010. She is currently pursuing the Ph.D. degree with the School of Electronics Engineering and Computer Science, Peking University. She was a Visiting Student with the Information Processing Laboratory, University of Washington, from 2012 to 2013. Her research interests include image/video coding and compressive sensing. She was a recipient of the best paper award of NCMT 2015.



**Yongbing Zhang** received the B.A. degree in English and the M.S. and Ph.D. degrees in computer science from the Harbin Institute of Technology, Harbin, China, in 2004, 2006, and 2010, respectively. He joined the Graduate School Shenzhen, Tsinghua University, Shenzhen, China, in 2010, where he is currently an Associate Research Fellow. His current research interests include video processing, image and video coding, video streaming, and transmission. He was a recipient of the Best Student Paper Award at the IEEE International Conference on Visual Communication and Image Processing in 2015.



**Siwei Ma** (S'03–M'12) received the B.S. degree from Shandong Normal University, Jinan, China, in 1999, and the Ph.D. degree in computer science from the Institute of Computing Technology, Chinese Academy of Sciences, Beijing, China, in 2005. From 2005 to 2007, he held a post-doctorate position with the University of Southern California, Los Angeles. Then, he joined the Institute of Digital Media, School of Electronics Engineering and Computer Science, Peking University, Beijing, where he is currently a Professor. He has authored over

100 technical articles in refereed journals and proceedings in the areas of image and video coding, video processing, video streaming, and transmission.



**Wen Gao** (M'92–SM'05–F'09) received the Ph.D. degree in electronics engineering from the University of Tokyo, Japan, in 1991. He was a Professor of Computer Science with the Harbin Institute of Technology from 1991 to 1995, and a Professor with the Institute of Computing Technology, Chinese Academy of Sciences. He is currently a Professor of Computer Science with Peking University, China. He has authored extensively, including five books and over 600 technical articles in refereed journals and

conference proceedings in the areas of image processing, video coding and communication, pattern recognition, multimedia information retrieval, multimodal interface, and bioinformatics. He served or serves on the Editorial Board for several journals, such as the IEEE TRANSACTIONS ON CIRCUITS AND SYSTEMS FOR VIDEO TECHNOLOGY, the IEEE TRANSACTIONS ON MULTIMEDIA, the IEEE TRANSACTIONS ON IMAGE PROCESSING, the IEEE TRANSACTIONS ON AUTONOMOUS MENTAL DEVELOPMENT, the *EURASIP Journal of Image Communications*, and the *Journal of Visual Communication and Image Representation*. He chaired a number of prestigious international conferences on multimedia and video signal processing, such as the IEEE ISCAS, ICME, and ACM Multimedia, and also served on the advisory and technical committees of numerous professional organizations.